# Ultrafast Exciton Transport with a Long Diffusion Length in Layered Perovskites with Organic Cation Functionalization

*Xun Xiao, Marvin Wu, Zhenyi Ni, Shuang Xu, Shangshang Chen, Jun Hu, Peter Neil Rudd, Wei You, and Jinsong Huang**

Layered perovskites have been employed for various optoelectronic devices including solar cells and light-emitting diodes for improved stability, which need exciton transport along both the in-plane and the out-of-plane directions. However, it is not clear yet what determines the exciton transport along the in-plane direction, which is important to understand its impact toward electronic devices. Here, by employing both steady-state and transient photoluminescence mapping, it is found that in-plane exciton diffusivities in layered perovskites are sensitive to both the number of layers and organic cations. Apart from exciton–phonon coupling, the octahedral distortion is revealed to significantly affect the exciton diffusion process, determined by temperature-dependent photoluminescence, light-intensity-dependent time-resolved photoluminescence, and density function theory calculations. A simple fluorine substitution to phenethylammonium for the organic cations to tune the structural rigidity and octahedral distortion yields a record exciton diffusivity of 1.91 $cm^2$ $s^{-1}$ and a diffusion length of 405 nm along the in-plane direction. This study provides guidance to manipulate exciton diffusion by modifying organic cations in layered perovskites.

Layered organic–inorganic hybrid perovskites are emerging as a star class of optoelectronic materials for efficient light-emitting diodes (LED), stable solar cells, sensitive photodetectors and X-ray detectors.[1–5] A general structure of $R_2A_{n-1}M_nX_{3n+1}$ is adopted in layered perovskites, where R is alkyl or aromatic amine cations as spacers to separate inorganic sheets, A is the organic cation, M is the metal ion and X is the halide. The variable n indicates the number of inorganic sheets sandwiched between two spacer cations.[6,7] Due to the dielectric

confinement from the organic cations, carriers in layered perovskite, especially for those with $n \leq 3$, are dominated by excitons with binding energies as high as hundreds of meV.[8–10] As binding energy of the excitons are much larger than the thermal energy at room temperature ($\approx$26 meV), we speculate that incident photons generate mainly excitons, and a small portion of free carriers,[11] though it is still very likely. In addition, it is intuitive that the out-of-plane carrier transport in layered perovskites is significantly weaker due to the much less conductive organic cations.[12–15] The measured mobility along the out-of-plane direction of $BA_2MA_2Pb_3I_{10}$ single crystals is in the order of $10^{-4}$ $cm^2$ $V^{-1}$ $s^{-1}$,[16] which is at least three orders magnitude smaller than that in corresponding 3D perovskites. One presumption that in-plane exciton transport is significantly faster has guided the design of efficient layered-perovskite-based devices by aligning the layers along the built-in electric field direction of the solar cells.[16–20] For instance, hot-casting and mixed solvent methods were reported to achieve an edge-on structure to enhance the carrier transport in layered perovskite solar cells.[10,21] In many other cases, 2D perovskites have been frequently introduced to passivate the grain boundaries and surface to enhance the stability of the perovskites films.[20,22] These layered perovskites still absorb a significant amount of light and generate excitons in the layers, while whether these excitons could be efficiently collected along the in-plane direction has not been answered yet. An empirical assumption that has always been made for exciton extraction in layered-perovskite-based devices: the in-plane transport in layered perovskite is sufficient for the excitons to reach the edge of layered perovskites where excitons dissociate into free charges by edge states, or 3D perovskites.[16,23] However this assumption has yet to be well confirmed. Recently, Deng et al. revealed that the exciton diffusivities for low-n-valued layered perovskite like $BA_2PbI_4$ ($n = 1$) and $BA_2MAPb_2I_7$ ($n = 2$) were only 0.06 and 0.07 $cm^2$ $s^{-1}$, respectively, at room temperature[24] which are about one order magnitude smaller than in 3D counterparts (0.54–1.2 $cm^2$ $s^{-1}$).[25–28] The corresponding in-plane exciton diffusion lengths were derived to be around 160 nm, which was much smaller than the film thickness ($\approx$400–500 nm) to absorb most of sun light within absorption spectral range.[20,24] Soon

X. Xiao, Dr. Z. Ni, S. Xu, Dr. S. Chen, P. N. Rudd, Prof. W. You, Prof. J. Huang
Department of Applied Physical Sciences
University of North Carolina at Chapel Hill
Chapel Hill, NC 27599, USA
E-mail: jhuang@unc.edu
Prof. M. Wu
Department of Physics
North Carolina Central University
Durham, NC 27707, USA
Dr. J. Hu, Prof. W. You
Department of Chemistry
University of North Carolina at Chapel Hill
Chapel Hill, NC 27599, USA

**ADVANCED
SCIENCE NEWS**
www.advancedsciencenews.com

**ADVANCED
MATERIALS**
www.advmat.de

after, Seitz et al. found the relations between the structural rigidity and exciton diffusivity, which suggests larger lattice stiffness would suppress exciton–phonon coupling and promote in-plane diffusion of excitons in $n = 1$ layered perovskites with an enhanced diffusion length of 236 nm.[28] However, the origin of the limitations for the layer-dependent carrier diffusion in layered perovskite has not yet been well explained, and solutions for tailoring the diffusivity as well as further prolonging exciton diffusion length in low-n-value layered perovskites are urgently needed.

Here, we systematically study the in-plane exciton diffusion in layered perovskite single crystals by tuning their organic cations and number of layers. Using steady-state and transient photoluminescence mapping (TPLM) to image the carrier diffusion in single-crystalline layered perovskites, we find the in-plane exciton diffusivity in layered perovskites are dependent on both number of layers and organic cations. With multiple analytical methods, it is confirmed that, in addition to exciton–phonon coupling, octahedral tilting of inorganic sheets is another dominant limitation to the in-plane diffusivity of layered perovskites. Finally, we find that by enhancing the interaction strength between organic cations, via a simple fluorine substitution in phenethylammonium (PEA$^+$) to give 3-fluoro-phenethylammonium (mF-PEA$^+$), could simultaneously suppress exciton–phonon coupling and release the out-of-plane octahedral tilting, leading to a record diffusivity of 1.91 cm$^2$ s$^{-1}$ and diffusion length of 405 nm. This work unveils the origins of the limited in-plane diffusion in layered perovskites, and provides guidance for manipulating exciton diffusivity through organic cation design.

The carrier diffusion dynamics in layered perovskites was studied by TPLM with the setup shown in **Figure 1**a (see Experimental Section for additional details). A 405 nm pulsed laser source with a repetition rate of 76 MHz was focused onto the sample surface by a 100× oil immersion objective. Considering the short wavelength of the excitation laser and the large numerical aperture (1.4 NA) of the lens, the excitation spot size could be reduced to the near-diffraction limit of ≈300 nm. Epifluorescence representative of the distribution of excited carriers was imaged onto a 30 μm pinhole through a 1.2× magnification relay lens system incorporating an x–y galvanometer. Light passing through the pinhole was then focused onto an avalanche photodiode (APD) for time-correlated single-photon counting. The angles of the galvanometer mirrors defines the region of the sample from which the light transmitted through the pinhole originates, and the x- and y-mirrors were scanned to create 2D maps of carrier diffusion. A longpass filter was placed before the APD to eliminate residual excitation light.

Thin single crystals of layered perovskites used in this study were grown by the recently developed space confined growth method.[29] The typical size of the layered perovskite single crystal is 2–4 mm laterally, and 1–10 μm in thickness.[29] The phase purity of the single-crystalline samples was verified by both their PL spectrum and X-ray diffraction (XRD) patterns as shown in Figure S1 (Supporting Information). The presence of only (00k) plane family in XRD suggests that the [PbI$_6$]$^{4-}$ octahedral layers are parallel to the substrate, providing an ideal platform to study the in-plane carrier transport.[28] Figure 1b shows the representative TPLM images for mF-PEA$_2$PbI$_4$ with time delays ranging from right after excitation to 400 ps. These TPLM images are normalized at each frame to highlight the time-dependent broadening of the PL mapping. As the time and spatial resolved PL intensity $I(x,y,t)$ could represent the exciton population $N(x,y,t)$, the growing PL distributions in TPLM images reflects the in-plane exciton transport in the layered perovskite. In addition, it shows that the exciton diffusion in the x–y plane is isotropic as the broadening speed of the PL emission spot are similar along both the x and y directions. The initial exciton population should follow the Gaussian distribution of the excitation beam.[24] At
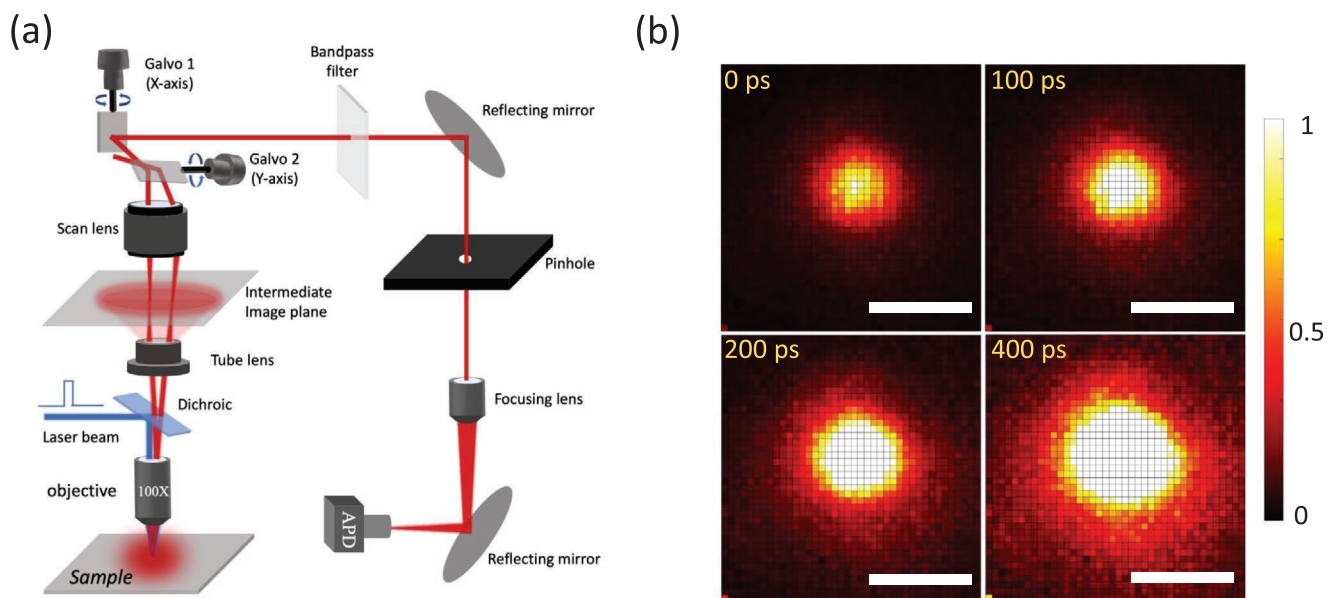


**Figure 1.** Transient photoluminescence mapping for in-plane exciton diffusion study. a) Setup for TPLM. b) Representative mF-PEA$_2$PbI$_4$ PL distribution mapping with time delay ranging from 0 to 400 ps after excitation. PL intensity is normalized at each time frame. The scale bar is 1 μm.
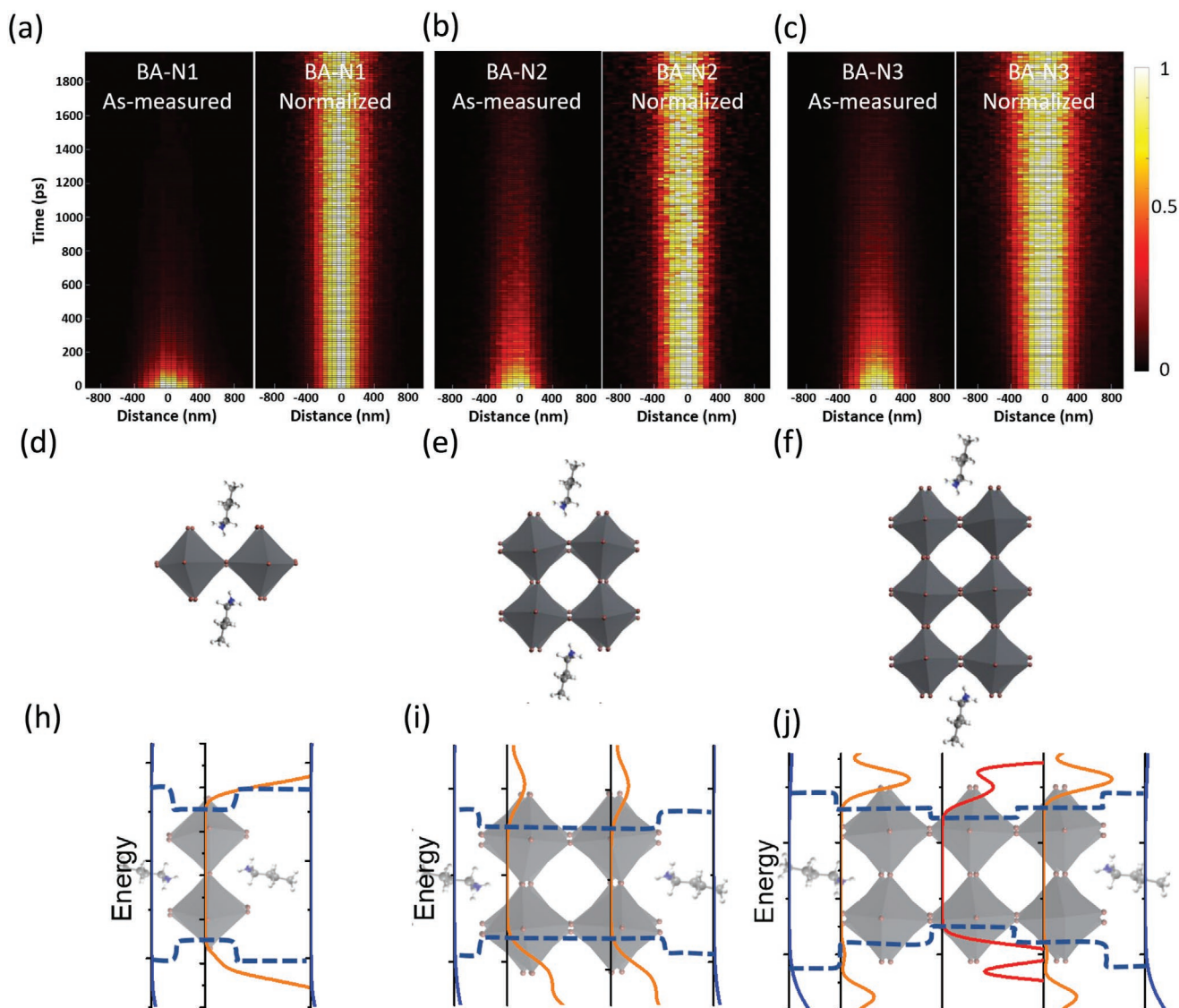
**2004080 (2 of 9)**

ADVANCED
SCIENCE NEWS
www.advancedsciencenews.com

ADVANCED
MATERIALS
www.advmat.de

**Figure 2.** Exciton diffusion in BA$^+$-based layered perovskites. a–c) As-measured/normalized diffusion maps for BA-N1, BA-N2, and BA-N3. The horizontal axis is the PL distribution along $x$-axis, the vertical axis is the time delay after excitation. "As-measured" means normalized with initial PL intensity. "Normalized" indicates normalized PL intensity at each frame. d–f) Cross-section view of the crystal structures of BA-N1 to BA-N3. h–j) Layer-by-layer energy diagrams imposed on the crystal structures.

a certain time delay ($t$) allowing for excitons to diffuse, the exciton population distribution could then be described as

$$N(x,y,t) = N_t \exp\left[-\frac{(x-x_0)^2}{2\sigma_t^2} - \frac{(y-y_0)^2}{2\sigma_t^2}\right].$$ Considering the iso-

tropic in-plane diffusion of excitons, investigation of the temporal 1D diffusion along the $x$-axis $N(x,0,t)$ is representative of the in-plane exciton diffusion process.[24,28] One prerequisite to apply this analysis is that the surface charge recombination is much weaker than bulk recombination, which is valid in the single crystals of the layered perovskites in this study.

We first employed TPLM on a family of butylammonium cation (BA$^+$)-based layered perovskite, BA$_2$PbI$_4$ (BA-N1), BA$_2$MAPb$_2$I$_7$ (BA-N2), and BA$_2$MA$_2$Pb$_3$I$_{10}$ (BA-N3). The excitation intensities were kept at $2.7 \times 10^{12}$ cm$^{-2}$, corresponding to an average bulk density of $5.2 \times 10^{16}$ cm$^{-3}$ within the absorption

length, below the estimated Mott density of $10^{14}$ cm$^{-2}$ and in the linear regime, to ensure PL signal proportional to the exciton density.[24,28,30] The diffusion mappings of BA-N1, BA-N2, and BA-N3 in **Figure 2**a–c show the broadening of PL distribution along the $x$-axis after excitation. For BA-N1 and BA-N2, the PL emission spots maintain a near constant size in the given time range, indicating a very limited number of excitons could diffuse out of the excitation spot. For BA-N3, more obvious broadening of the temporal and spatial PL distribution is observed, suggesting a larger exciton diffusivity in BA-N3. The exact exciton diffusivity ($D$) could be derived with $D = \frac{\sigma_t^2 - \sigma_0^2}{2t}$, where $\sigma_t^2$ is mean-square-distribution of PL at a time delay of $t$ and $\sigma_0^2$ is the initial mean-square-distribution at $t = 0$. By extracting the $\sigma_t^2$ from the PL distribution within 500 ps time delay after excitation, the diffusivities are determined to be

0.058 ± 0.005, 0.067 ± 0.007, and 0.121± 0.02 cm² s⁻¹ for BA-N1, BA-N2, and BA-N3 (Figure S2, Supporting Information), respectively, which is consistent with reported values.[24] The exciton lifetimes ($\tau$) are determined from the PL decay time of fast process in biexponential model, since it includes the majority of the emission photons. Combining the derived diffusivities ($D$) and exciton lifetime ($\tau$), the respective diffusion lengths for BA-N1, BA-N2, and BA-N3 are calculated, with $L_D = \sqrt{2D\tau}$,[24,25,28] to be 50.9 ± 2.1, 56.1 ± 3.2, and 101.2 ± 7.5 nm. It is worth mentioning, diffusivities in BA-N1 and N2 almost reach the minimum diffusivity limit with our current TPLM setup. The steady-state PL mapping were conducted with the setup shown in Figure S3a (Supporting Information). The 473 nm CW laser with an excitation power of 5.95 W cm⁻², which induced an exciton density of 2.3 × 10¹³ cm⁻³ due to the short exciton recombination lifetime, was applied to generate excitons. As the excitation spot was fixed, the PL intensity of the surrounding area representative for the exciton population after diffusion was collected by a scanning APD which integrated steady-state PL signals from the selected wavelength range. As a result, the steady-state PL mappings for BA-N1 and BA-N2 showed emission spot close to the excitation size (Figure S3b–d, Supporting Information), which verified the limited exciton diffusivities in BA-N1 and BA-N2. The broader emission spot sizes in steady-state PL mapping of BA-N3 as well as referenced MAPbI₃ (3D) further confirmed the improved in-plane diffusion length with increasing number of layers to BA-N3 (Figure S3e,f, Supporting Information). The poor exciton diffusivity and diffusion length indicated that excitons in BA⁺-based layered perovskites cannot easily diffuse to the edge of layers.

To find out the origin of the layer-dependent diffusivity in BA⁺-based layered perovskites, we examined three possible reasons: defects/traps, exciton–phonon coupling and structural differences (octahedral tilting). Some defects in perovskites can cause localized states in the forbidden gap which trap charges and excitons.[31] In addition, trap states are observed to slow exciton diffusion for the time delay of a few nanoseconds or longer after excitation in layered perovskite systems.[27] To check whether trap states play a critical role in these single-crystal samples, light-intensity-dependent time-resolved PL (TRPL) measurements were carried out with light fluences ranging from 2.21 × 10¹¹ to 2.21 × 10¹³ cm⁻², corresponding to the exciton density from 7.3 × 10¹⁵ to 7.3 × 10¹⁷ cm⁻³. If there

were abundant trap states, the carrier recombination dynamics at low excitation intensities would be dominated by the trapping/de-trapping process.[32] In contrast, at a high excitation intensity, the recombination dynamics would then be determined by bimolecular recombination or Auger recombination as the trap states could be filled.[32] Since bimolecular recombination is much faster than trapping/de-trapping process, the TRPL lifetime would be longer at a low excitation intensity for samples with abundant charge traps. However, no obvious recombination lifetime change in recombination lifetimes for all BA-based layered perovskites are observed over various light intensities, as shown in Figure S4 (Supporting Information). This indicates that trap states did not play a significant role in the comparison of these samples with the light fluence ranging from 7.3 × 10¹⁵ to 7.3 × 10¹⁷ cm⁻³. Considering the fluence used in TPLM (5.2 × 10¹⁶ cm⁻³) was also in this range, trap states cannot explain the observed variation in diffusivity for the BA-based layered perovskite family. It is possible that trap states would slow the excitons diffusion when exciton density has greatly dropped to be comparable to trap density, i.e., >2 ns after excitation as observed by Seitz et, al.[28] The diffusion mapping here was collected within 1.8 ns after excitation to derive the diffusivities, which should not be significantly affected by the trap states.

In addition to trap states, exciton–phonon coupling has been reported to strongly affect exciton dynamics in layered perovskites.[33,34] Phonon scattering is one of the common scattering mechanisms that reduces the carrier mean drift time and lowers the diffusivity. As a consequence of the lattice vibration, exciton–phonon coupling usually gets suppressed when the lattice becomes more rigid and has lower phonon densities. One reported method to quantify the exciton–phonon coupling strength is measuring the temperature-dependent PL linewidth broadening.[35] Here we measured the temperature-dependent PL linewidth for BA⁺-based layered perovskites from 260 to 300 K as a phase transition was observed below 250 K for the BA-N1 sample. The phase transition is confirmed by temperature-dependent XRD and PL spectra (Figure S5, Supporting Information). Each data point was collected by extracting the PL linewidth from three individual samples to avoid the influence of sample variation. Analyzing the statistical results at various temperatures, the exciton–phonon coupling strength were derived to be 22.02 ± 3.23, 21.93 ± 1.51, and 22.25 ± 1.71 meV for BA-N1, BA-N2, and BA-N3, respectively (**Table 1** and Figure S6,

**Table 1.** Summary of exciton–phonon coupling strength, octahedral tilting and diffusivities for various layered perovskites.

| Composition | Exciton–phonon coupling strength [meV] | Out-of-plane tilting angle [°] | In-plane tilting angle [°] | Diffusivity [cm² s⁻¹] | Diffusion length [nm] |
|---|---|---|---|---|---|
| BA-N1 | 22.02 ± 3.23 | 4.8 | 34.6 | 0.058 ± 0.005 | 50.9 ± 2.1 |
| BA-N2 | 21.93 ± 1.51 | 10.3 | 1.4 | 0.067 ± 0.007 | 56.1 ± 3.2 |
| BA-N3 | 22.25 ± 1.71 | 3.6 (middle layer) | 0.2 (three layers) | 0.121 ± 0.02 | 101.2 ± 7.5 |
|  |  | 10.7 (surface layer) |  |  |  |
| PEA-N1 | 12.71 ± 0.06 | 1.8 | 38.4 | 0.648 ± 0.05 | 227.7 ±11.2 |
| PEA-N2 | 13.51 ± 0.13 | 25.8 | 9.2 | 0.157 ± 0.005 | 92.4 ± 1.7 |
| PEA-N3 | 14.96 ± 0.15 | 2.5 (middle layer) | 8.6 (three layers) | 0.189 ± 0.008 | 137.5 ± 2.1 |
|  |  | 9.5 (surface layer) |  |  |  |
| mF-PEA-N1 | 11.38 ± 0.15 | 0.7 | 37.3 | 1.91 ± 0.09 | 405 ± 13.5 |

Supporting Information). As a result, negligible difference of exciton–phonon coupling strength among BA-N1, BA-N2, and BA-N3 could be observed, meaning that the exciton–phonon coupling unlikely dominates the observed difference in diffusivity.

The structural differences among the three types of layered perovskites in BA+ family were then investigated, especially for the octahedral tilting proved to have a significant impact on the effective mass of carriers and thus carrier mobility.[36] Inspired by the anisotropic structures of the layered perovskites, the in-plane and out-of-plane tilting are analyzed. Here, the in-plane tilting is defined as the difference between 180° and the Pb—I—Pb bond angle by projecting the bridging I atoms onto the plane of Pb atoms.[37] The out-of-plane tilting describes the shift of Pb—I bonds away from the normal direction of the plane of Pb atoms, as illustrated in Figure S7 (Supporting Information). Both in-plane and out-of-plane tilting have been determined to greatly influence the orbital overlapping of octahedra.[37] A larger tilting angle would increase the orbital overlapping and result in a loss of antibonding interactions, for instance, between the s orbitals of the metal and the $p_x$ and $p_y$ orbitals in halide, which would lower valence band maximum and enlarge the bandgap.[38] Moreover, a larger tilting angle has also been revealed to increase the effective mass for both electrons and holes, and thus lower the diffusivity.[36] Indexing the crystal structures from single-crystal XRD,[39,40] the out-of-plane tilting angles are determined to be 4.8° and 10.3° for BA-N1 and BA-N2, respectively. The increased out-of-plane tilting in BA-N2 might come from the nonsymmetrical distribution of methylammonium cation (MA+) and BA+ on both sides of the octahedral layer, compared with BA-N1 whose octahedral layer is connected with the same organic cations, BA+, at both sides. Different organic cations with various steric effects likely have different penetration depths of the ammonium into the octahedral layer as well as altered head orientation, influencing the interaction strength between organic cation and octahedral.[37] As a consequence, the un-balanced interaction strength would distort the octahedral and cause the out-of-plane tilting. For BA-N3, both the surface octahedral layers show the out-of-plane tilting angle of 10.7° which is much larger than 3.6° in the middle layer. This could be explained as the surface layers are experiencing un-balanced interaction strength from different attached cations (MA+ and BA+) like BA-N2, while the middle layer has same cations on both sides. The incorporation of MA+ would also introduce a competition between the two cations to meet their stereochemical requirements,[40] and both BA+ and MA+ would be displaced from their preferred orientations and mitigate the in-plane tilting. As a result, the in-pane tilting angle decreased from 34.6° in BA-N1 to 1.4° in BA-N2 and <0.5° in the three octahedral slabs for BA-N3. Density function theory (DFT) calculations were conducted to determine the energy band diagrams with respect to the crystal structures, as shown in Figure 2h–j. BA-N1 and BA-N2 exhibit a flat band structure across different perovskite slabs. As for BA-N3, an energy confinement quantum well band structure within the three octahedral layers is observed, which should result from larger out-of-plane tilting of the surface layers resulting in a larger bandgap while the flatter middle layer possesses a relatively smaller bandgap.[38] Considering both the in-/out-of- plane

tilting would influence exciton transport, the severe in-plane tilting in BA-N1 and large out-of-plane tilting in BA-N2 would limit diffusivities in these two types of layered perovskites, while energy confinement within BA-N3 perovskite slabs guarantees a higher exciton diffusivity along the less-distorted middle layer with higher diffusivity of the BA-N3.

We then applied TPLM on PEA+-based layered perovskites. A PL intensity enhancement was observed by replacing BA+ with PEA+ in the steady-state PL measurement with same excitation condition (Figure S8, Supporting Information), which indicated a PL quantum yield increase. It should come from larger lattice rigidity that suppress exciton–phonon coupling strength and nonradiative recombination process.[28,33] The respective diffusion mappings for $PEA_2PbI_4$ (PEA-N1), $PEA_2MAPb_2I_7$ (PEA-N2), and $PEA_2MA_2Pb_3I_{10}$ (PEA-N3) are shown in **Figure 3**a–c. Compared with BA+-based layered perovskites, PEAI-based layered perovskites exhibit much clearer temporal broadening of PL emission spot sizes, which indicates larger diffusivities for in-plane exciton diffusion. Deriving D from the time-dependent mean-square-distribution width ($\sigma_t^2$) as shown in Figure 3d results in diffusivities of 0.648 ± 0.05, 0.157 ± 0.005, and 0.189 ± 0.008 cm² s⁻¹ for PEA-N1, PEA-N2, and PEA-N3, respectively (Figure 3e). The significantly enhanced exciton diffusivity in PEA-N1 compared with BA-N1 is consistent with the previous reports,[28] which should be due to the suppressed exciton–phonon coupling with more rigid PEAI molecular as the organic spacer. The much smaller atomic displacement in PEA-N1 further confirmed the enhanced lattice rigidity compared with BA+-based layered perovskites, which should result from pi-hydrogen bonds between the aromatic rings of the cations (Figure S9, Supporting Information). The corresponding diffusion lengths were calculated to be 227.7 ± 11.2, 92.4 ± 1.7, and 137.5 ± 2.1 nm for PEA-N1, PEA-N2, and PEA-N3, which were improved compared with BA+-based layered perovskites and in line with previous reports.[28] However, they were still much smaller than the desired film thickness (≈400–500 nm) for efficient perovskite solar cells.[20,24] Nevertheless, it should be noted that in BA+-based layered perovskites, the exciton diffusivity gradually increased from BA-N1 to BA-N3; however, when increasing the number of octahedral slabs in PEAI family, the diffusivity first dropped dramatically by about 75% from PEA-N1 to PEA-N2, and then increased around 20% from PEA-N2 to PEA-N3.

To understand the diffusivity evolution in PEA+-based perovskites, we also systematically checked the three possibilities: defects/trap states, exciton–phonon coupling and structural difference (octahedral tilting). The PL recombination lifetimes for all three PEA+-based layered perovskites proved to be insensitive to changes in light fluences varying from $7.3 \times 10^{15}$ to $7.3 \times 10^{17}$ cm⁻³ as well, indicating that trap states do not play a significant role in the observed diffusivity variation of these crystals (Figure S10, Supporting Information). The exciton–phonon coupling strengths were also extracted with temperature-dependent PL linewidth broadening method (Figure S11, Supporting Information), and found to be 12.71 ± 0.06, 13.51 ± 0.13, and 14.96 ± 0.15 meV for PEA-N1, PEA-N2, and PEA-N3, respectively. The suppressed exciton–phonon coupling with PEAI as the organic spacer agrees well with previous results,[33] and the elevating trend of the coupling strength from PEA-N1
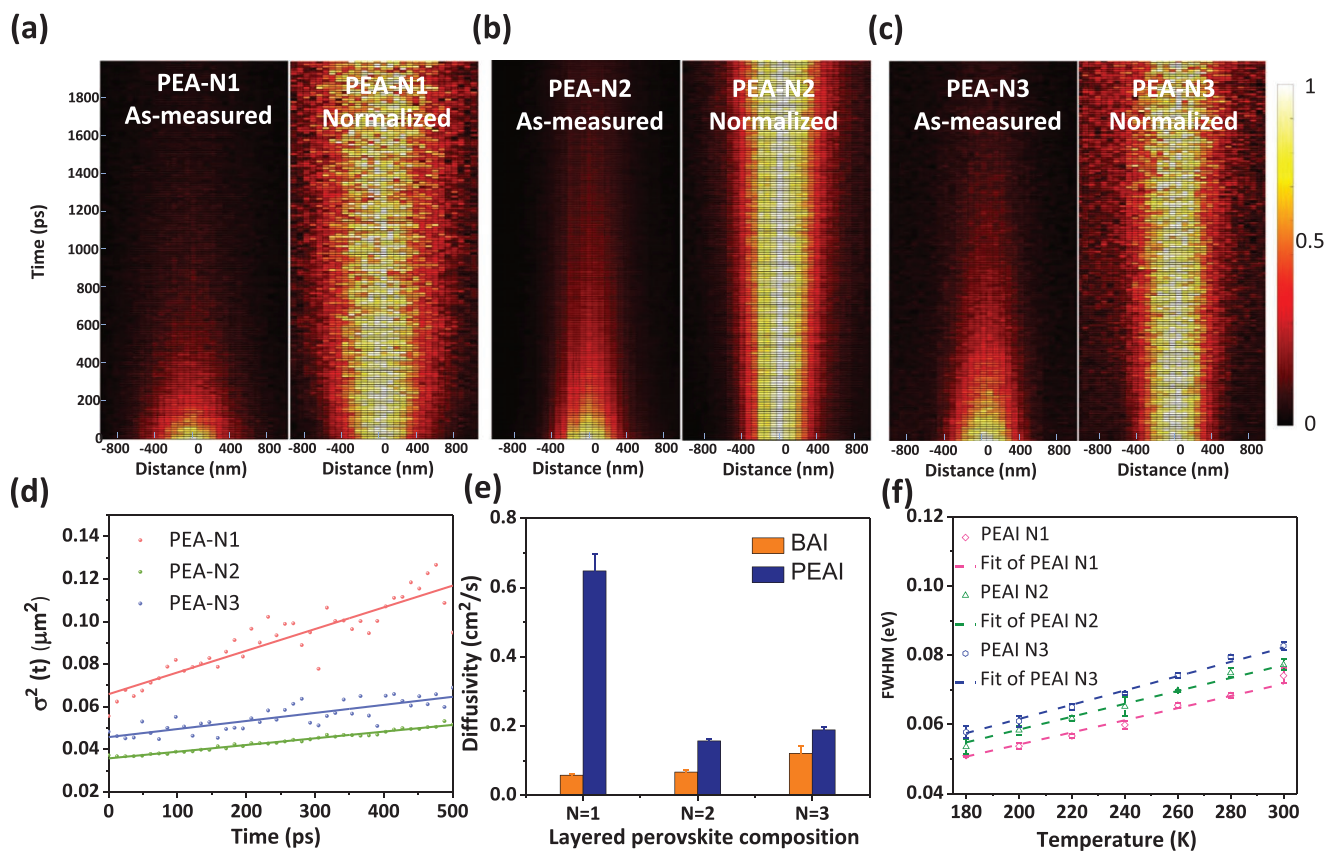
**Figure 3.** Exciton diffusion in PEA$^+$-based layered perovskites. a–c) As-measured/normalized diffusion maps for PEA-N1, PEA-N2, and PEA-N3. d) Time-dependent mean-square-distribution for PL emission spot broadening. e) Diffusivity comparison between BA$^+$- and PEA$^+$-based layered perovskites. The error bars represent 95% confidence intervals of the diffusivity fitting. f) Temperature-dependent PL linewidth (FWHM) of PEA-N1, PEA-N2 and PEA-N3.

to PEA-N3 should come from the softer lattice when incorporating more MA$^+$ molecules. Although the exciton–phonon coupling would affect the exciton transport, the increasing trend of the coupling strength cannot explain the initial drop in diffusivity followed by an increase seen when going from PEA-N1 to PEA-N3.

The structural differences were then investigated by extracting the in-plane/out-of-plane tilting angles from the crystal structures.[37] For the in-plane tilting angle, a large in-plane distortion (38.4°) is observed in PEA-N1 structure. This value is reduced to less than 10° in PEA-N2 and PEA-N3, which is similar than that of the BA$^+$ system. The out-of-plane tilting angles are extracted to be 1.8° for PEA-N1, 25.8° for PEA-N2, and 9.5° for the surface and 2.5° for the middle layers of PEA-N3, respectively. The much larger out-of-plane tilting angle in PEA-N2 should result from the severe difference in interaction strength between the octahedra with the PEA$^+$ and MA$^+$ cations. The larger distortion of the surface layers in PEA-N3 is also observed, resulting in a similar energy confinement band structure within the octahedral slabs. Due to the lowest exciton–phonon coupling strength and small out-of-plane distortion in PEA-N1 single crystals among the PEAI layered perovskites family, an impressive exciton diffusivity of 0.648 ± 0.05 cm$^2$ s$^{-1}$ is achieved, which is then comparable with that of MAPbI$_3$ single crystal (0.54–1.2 cm$^2$ s$^{-1}$).[25–28] The large in-plane tilting angle in PEA-N1 indicates that the diffusivity could be further

improved by mitigating the in-plane distortion. The significantly drop of the diffusivity (75%) from PEA-N1 to PEA-N2 can be attributed to the severe out-of-plane distortion coupled with the increased exciton–phonon coupling strength in PEA-N2. The 20% increase of the exciton diffusivity from PEA-N2 to PEA-N3 should come from the faster exciton diffusion along the less distorted middle layer in PEA-N3, even if the electron-phonon coupling strength get increased. After systematically studying the BA$^+$- and PEA$^+$-based layered perovskites, we confirmed the impact from both exciton–phonon coupling and octahedral in-/out-of- plane tilting on determining the exciton diffusivities in layered perovskites.

In addition to unveil the limitations of exciton diffusion in layered perovskites, strategies for manipulating exciton diffusivity to meet various devices requests are also explored. Although it is quite difficult to quantify the impacts from either exciton–phonon coupling or octahedral tilting on the exciton diffusivity, both limiting factors have been revealed to largely rely on the molecular design of the organic cations in layered perovskites. To reduce the exciton–phonon coupling, rigid cations that enhance the crystal stiffness could be adopted. Moreover, larger interaction strength of organic spacer tails between layers when octahedra slabs stacking together, like introducing stronger dipole-dipole force and pi-pi force between benzene rings in PEA$^+$ cations instead of weak van der Waals force between alkyl chains in BA$^+$
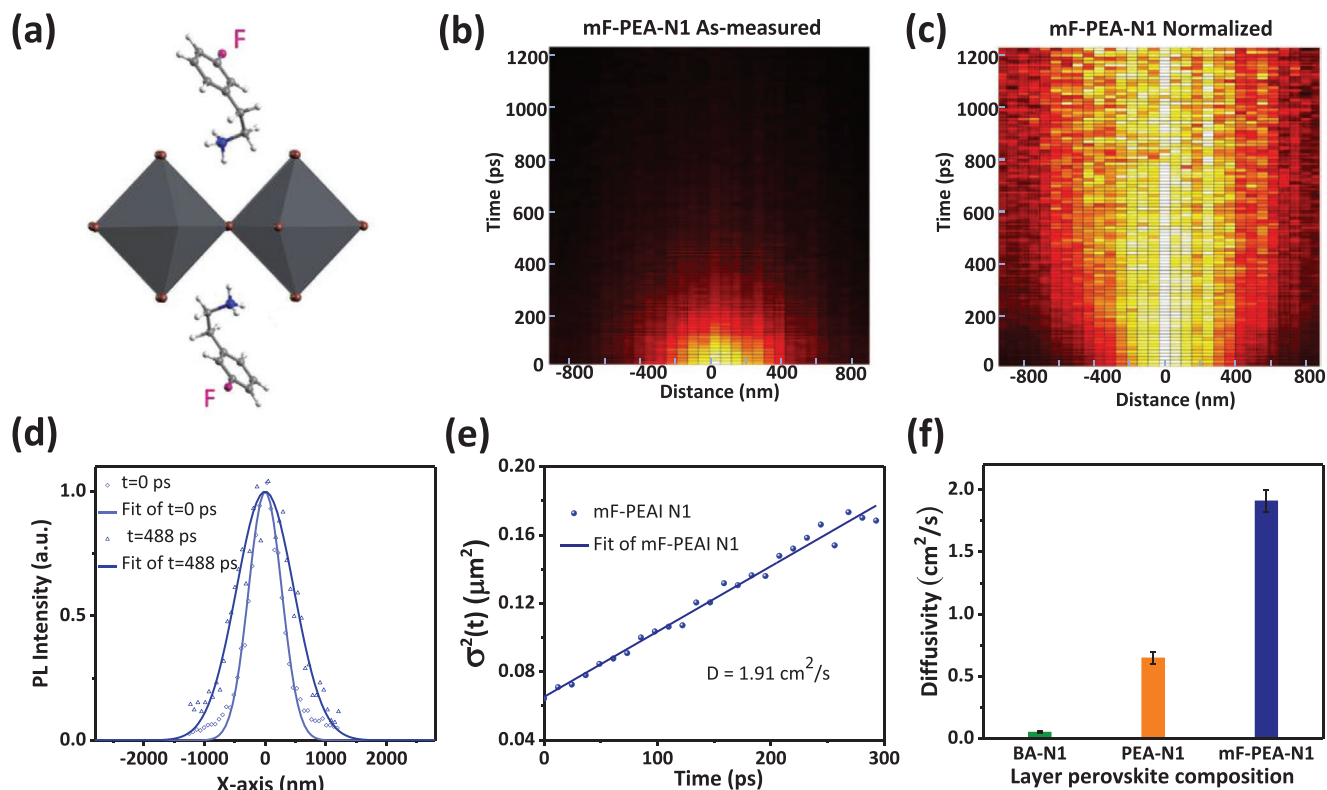
**Figure 4.** Exciton diffusion in mF-PEA-N1. a) Crystal structure of mF-PEA-N1.[41] b,c) As-measured and normalized diffusion maps for mF-PEA-N1. d) PL distribution along x-axis with 0 and 488 ps time delay after excitation. e) Time-dependent mean-square-distribution of PL emission spot. f) Comparison of diffusivities inBA-N1, PEA-N1, and mF-PEA-N1. The error bars represent 95% confidence intervals of the diffusivity fits.

cations, might help to mitigate the out-of-plane distortion by suppressing the displacement of ammonium head.[40] The displacement of ammonium head would change the interaction strength between organic cations and octahedra and induce the out-of-plane distortion, particularly for the cases with one octahedral slab. To achieve this and elevate exciton diffusivity, the PEAI molecular was modified with a simple fluorine substitution to make mF-PEAI.[41] Utilizing the modified mF-PEAI as the organic cation, single-crystalline mF-PEA$_2$PbI$_4$ (mF-PEA-N1) layered perovskite was synthesized. The crystal structure and corresponding XRD pattern were shown in **Figure 4**a and Figure S12, Supporting Information, respectively.[41,42] The fluorine substitution in mF-PEA$^+$ compared with PEA$^+$ would improve dipole strength of the molecules as well as the dipole–dipole interaction strength of the cation tails, which was confirmed in previous reports.[41,42] Hence, adopting mF-PEA$^+$ as organic spacer with stronger interaction strength between the cation tails allows for both a more compact and rigid lattice to reduce exciton–phonon coupling and a mitigation of out-of-plane distortion of octahedra by suppressing ammonium head displacement. The increased rigidity for mF-PEA-N1 is verified by the exciton–phonon coupling strength being suppressed to 11.38 ± 0.15 meV (Figure S13, Supporting Information) and the out-of-plane tilting angle being reduced to just 0.7° compared to 1.8° in PEA-N1 and 4.8° in BA-N1. The as-measured and normalized diffusion maps for mF-PEA-N1 are presented in Figure 4b–c. The fast exciton diffusion could be clearly observed from the temporal broadening of the PL

distribution (Figure 4d). The diffusivity ($D$) derived from $\sigma_t^2$ is 1.91 ± 0.09 cm$^2$ s$^{-1}$, which is increased by almost 190% compared to PEA-N1 and is the record for the known layered perovskites (Figure 4e,f).[24,28] This suggests that tuning dipole strength of the organic cations might be a feasible way to manipulate the in-plane exciton diffusivity in layered perovskites by varying the interaction strength of organic cation tails between layers when octahedral layers stacking together. The exciton diffusion length is calculated to be 405 ± 13.5 nm, which is also comparable with film thickness in the layered-perovskite-based devices.[10] This indicates that in-plane transport in mF-PEA-N1 should be sufficient for excitons to reach the layer edge and then get collected.

In conclusion, we have studied the exciton diffusion in various layered perovskites via TPLM and systematically studied the limitation factors of their exciton diffusivity through multiple analytical methods including light-intensity-dependent TRPL, temperature-dependent PL line width broadening and DFT calculation. It is revealed that apart from exciton–phonon coupling, the octahedral in-/out-of- plane tilting also plays a dominant role in determining exciton diffusivity. The exciton–phonon coupling is governed by the lattice rigidity, while the out-of-plane tilting of octahedral slabs relates to the interaction strength between the octahedra and organic cations. Through manipulating both lattice rigidity and out-of-plane tilting of the octahedra by a simple fluorine substitution of PEAI, we realized a record exciton diffusivity in layered perovskites of 1.91 cm$^2$ s$^{-1}$ and an enhanced diffusion

length of 405 nm, which further highlights the importance of organic cation design on manipulating exciton diffusion in layered perovskites.

## Experimental Section

*Thin Single-Crystal Growth*: The raw materials of BA/PEA, $CH_3NH_3I$, and $PbI_2$ are purchased from Sigma-Aldrich, then mixed with different stoichiometric ratios (2: 0: 1 for N1, 2: 1: 2 for N2, and 2: 2:3 for N3). The mixture was then dissolved in HI solution heated at 130 °C for 1 h to get a clear solution. The solution was then inserted into two cover glass on the hotplate at 130 °C. The temperature was decreased to room temperature gradually and crystals would grow between two substrates.

*TPLM Measurement*: Diffusion measurements were performed with a home-built inverted microscope. Samples were excited with the 80 fs, 405 nm output of a frequency doubled $Ti:Al_2O_3$ laser (Spectra Physics Tsunami) at a 76 MHz repetition rate. The excitation beam is focused through a 100×, 1.4 NA oil immersion objective (Olympus UPLSAPO), and photoluminescence was collected through the same objective. The emitted light is relayed using a 4f 1:1 tube lens–scan lens system onto an $x$–$y$ galvanometer (Thorlabs), and then focused onto a 30 μm pinhole with a net 120× magnification. The transmitted light is imaged onto a single-photon-counting avalanche photodiode (ID Quantique ID100-50, ultralow noise version), and time-correlated single-photon counting is performed by a Becker and Hickl SPC-130 module triggered by a portion of the excitation beam. The collection spot was scanned by computer-controlled rotation of the galvanometer mirrors with a step size of 61 nm. The temporal resolution of the system is 35 ps which is determined from measurements of scattered excitation light.

*Temperature-Dependent Photoluminescence Measurement*: Layered perovskite samples were attached to a portable LINKAM thermal stage to acquire PL spectrum with iHR320. The exciton–phonon coupling strength was derived from FWHM of PL spectra under various temperature with the equation

$$\Gamma\,(T) = \Gamma_0 + \frac{\Gamma_1}{\exp\left(\frac{\hbar\omega_1}{k_BT}\right)-1} \tag{1}$$

where $\Gamma_0$ is a temperature-independent inhomogeneous broadening term for imperfection scattering, $\Gamma_1$ represents the exciton–phonon coupling strength, contributed by longitudinal optical phonon scattering, and $\omega_1$ is the homopolar phonon frequency.

## Supporting Information

Supporting Information is available from the Wiley Online Library or from the author.

## Acknowledgements

## Conflict of Interest

The authors declare no conflict of interest.

[1] G. Grancini, C. Roldán-Carmona, I. Zimmermann, E. Mosconi, X. Lee, D. Martineau, S. Narbey, F. Oswald, F. De Angelis, M. Graetzel, M. K. Nazeeruddin, *Nat. Commun.* **2017**, *8*, 15684.

[2] W. Peng, J. Yin, K.-T. Ho, O. Ouellette, M. De Bastiani, B. Murali, O. El Tall, C. Shen, X. Miao, J. Pan, E. Alarousu, H. He Jr., B. S. Ooi, O. F. Mohammed, E. Sargent, O. M. Bakr, *Nano Lett.* **2017**, *17*, 4759.

[3] L. N. Quan, M. Yuan, R. Comin, O. Voznyy, E. M. Beauregard, S. Hoogland, A. Buin, A. R. Kirmani, K. Zhao, A. Amassian, D. H. Kim, E. H. Sargent, *J. Am. Chem. Soc.* **2016**, *138*, 2649.

[4] M. Yuan, L. N. Quan, R. Comin, G. Walters, R. Sabatini, O. Voznyy, S. Hoogland, Y. Zhao, E. M. Beauregard, P. Kanjanaboos, Z. Lu, D. H. Kim, E. H. Sargent, *Nat. Nanotechnol.* **2016**, *11*, 872.

[5] L. Zhang, X. Yang, Q. Jiang, P. Wang, Z. Yin, X. Zhang, H. Tan, Y. Yang, M. Wei, B. R. Sutherland, E. H. Sargent, J. You, *Nat. Commun.* **2017**, *8*, 15640.

[6] S. Aharon, L. Etgar, *Nano Lett.* **2016**, *16*, 3230.

[7] J. Liu, Y. Xue, Z. Wang, Z.-Q. Xu, C. Zheng, B. Weber, J. Song, Y. Wang, Y. Lu, Y. Zhang, Q. Bao, *ACS Nano* **2016**, *10*, 3536.

[8] D. H. Cao, C. C. Stoumpos, O. K. Farha, J. T. Hupp, M. G. Kanatzidis, *J. Am. Chem. Soc.* **2015**, *137*, 7843.

[9] D. B. Mitzi, *Chem. Mater.* **1996**, *8*, 791.

[10] H. Tsai, W. Nie, J.-C. Blancon, C. C. Stoumpos, R. Asadpour, B. Harutyunyan, A. J. Neukirch, R. Verduzco, J. J. Crochet, S. Tretiak, L. Pedesseau, J. Even, M. A. Alam, G. Gupta, J. Lou, P. M. Ajayan, M. J. Bedzyk, M. G. Kanatzidis, A. D. Mohite, *Nature* **2016**, *536*, 312.

[11] M. C. Gélvez-Rueda, E. M. Hutter, D. H. Cao, N. Renaud, C. C. Stoumpos, J. T. Hupp, T. J. Savenije, M. G. Kanatzidis, F. C. Grozema, *J. Phys. Chem. C* **2017**, *121*, 26566.

[12] J.-C. Blancon, A. V. Stier, H. Tsai, W. Nie, C. C. Stoumpos, B. Traoré, L. Pedesseau, M. Kepenekian, F. Katsutani, G. T. Noe, J. Kono, S. Tretiak, S. A. Crooker, C. Katan, M. G. Kanatzidis, J. J. Crochet, J. Even, A. D. Mohite, *Nat. Commun.* **2018**, *9*, 2254.

[13] M. Li, Q. Wei, S. K. Muduli, N. Yantara, Q. Xu, N. Mathews, S. G. Mhaisalkar, G. Xing, T. C. Sum, *Adv. Mater.* **2018**, *30*, 1707235.

[14] O. Yaffe, A. Chernikov, Z. M. Norman, Y. Zhong, A. Velauthapillai, A. Van Der Zande, J. S. Owen, T. F. Heinz, *Phys. Rev. B* **2015**, *92*, 045414.

[15] Y. Lin, Y. Bai, Y. Fang, Q. Wang, Y. Deng, J. Huang, *ACS Energy Lett.* **2017**, *2*, 1571.

[16] Y. Lin, Y. Fang, J. Zhao, Y. Shao, S. J. Stuard, M. M. Nahid, H. Ade, Q. Wang, J. E. Shield, N. Zhou, A. M. Moran, J. Huang, *Nat. Commun.* **2019**, *10*, 1008.

[17] X. Wu, M. T. Trinh, X.-Y. Zhu, *J. Phys. Chem. C* **2015**, *119*, 14714.

[18] C. M. Mauck, W. A. Tisdale, *Trends Chem.* **2019**, *1*, 380.

[19] A. Z. Chen, M. Shiu, J. H. Ma, M. R. Alpert, D. Zhang, B. J. Foley, D.-M. Smilgies, S.-H. Lee, J. J. Choi, *Nat. Commun.* **2018**, *9*, 1336.

[20] Z. Wang, Q. Lin, F. P. Chmiel, N. Sakai, L. M. Herz, H. J. Snaith, *Nat. Energy* **2017**, *2*, 17135.

[21] C. M. M. Soe, W. Nie, C. C. Stoumpos, H. Tsai, J.-C. Blancon, F. Liu, J. Even, T. J. Marks, A. D. Mohite, M. G. Kanatzidis, *Adv. Energy Mater.* **2018**, *8*, 1700979.

[22] Y. Chen, Y. Sun, J. Peng, J. Tang, K. Zheng, Z. Liang, *Adv. Mater.* **2018**, *30*, 1703487.

**ADVANCED
SCIENCE NEWS**

www.advancedsciencenews.com

**ADVANCED
MATERIALS**

www.advmat.de

[23] J.-C. Blancon, H. Tsai, W. Nie, C. C. Stoumpos, L. Pedesseau, C. Katan, M. Kepenekian, C. M. M. Soe, K. Appavoo, M. Y. Sfeir, S. Tretiak, P. M. Ajayan, M. G. Kanatzidis, J. Even, J. J. Crochet, A. D. Mohite, *Science* **2017**, *355*, 1288.

[24] S. Deng, E. Shi, L. Yuan, L. Jin, L. Dou, L. Huang, *Nat. Commun.* **2020**, *11*, 664.

[25] M. I. Saidaminov, K. Williams, M. Wei, A. Johnston, R. Quintero-Bermudez, M. Vafaie, J. M. Pina, A. H. Proppe, Y. Hou, G. Walters, S. O. Kelley, W. A. Tisdale, E. H. Sargent, *Nat. Mater.* **2020**, *19*, 412.

[26] A. H. Hill, C. L. Kennedy, E. S. Massaro, E. M. Grumstrup, *J. Phys. Chem. Lett.* **2018**, *9*, 2808.

[27] Q. Dong, Y. Fang, Y. Shao, P. Mulligan, J. Qiu, L. Cao, J. Huang, *Science* **2015**, *347*, 967.

[28] M. Seitz, A. J. Magdaleno, N. Alcázar-Cano, M. Meléndez, T. J. Lubbers, S. W. Walraven, S. Pakdel, E. Prada, R. Delgado-Buscalioni, F. Prins, *Nat. Commun.* **2020**, *11*, 2035.

[29] X. Xiao, J. Dai, Y. Fang, J. Zhao, X. Zheng, S. Tang, P. N. Rudd, X. C. Zeng, J. Huang, *ACS Energy Lett.* **2018**, *3*, 684.

[30] J. P. Philbin, E. Rabani, *Nano Lett.* **2018**, *18*, 7889.

[31] H. Jin, E. Debroye, M. Keshavarz, I. G. Scheblykin, M. B. J. Roeffaers, J. Hofkens, J. A. Steele, *Mater. Horiz.* **2020**, *7*, 397.

[32] M. Maiberg, T. Hölscher, S. Zahedi-Azad, R. Scheer, *J. Appl. Phys.* **2015**, *118*, 105701.

[33] X. Gong, O. Voznyy, A. Jain, W. Liu, R. Sabatini, Z. Piontkowski, G. Walters, G. Bappi, S. Nokhrin, O. Bushuyev, M. Yuan, R. Comin, D. Mccamant, S. O. Kelley, E. H. Sargent, *Nat. Mater.* **2018**, *17*, 550.

[34] Z. Guo, X. Wu, T. Zhu, X. Zhu, L. Huang, *ACS Nano* **2016**, *10*, 9992.

[35] S. Rudin, T. L. Reinecke, B. Segall, *Phys. Rev. B* **1990**, *42*, 11218.

[36] J.-H. Lee, N. C. Bristowe, J. H. Lee, S.-H. Lee, P. D. Bristowe, A. K. Cheetham, H. M. Jang, *Chem. Mater.* **2016**, *28*, 4259.

[37] K.-Z. Du, Q. Tu, X. Zhang, Q. Han, J. Liu, S. Zauscher, D. B. Mitzi, *Inorg. Chem.* **2017**, *56*, 9291.

[38] J. L. Knutson, J. D. Martin, D. B. Mitzi, *Inorg. Chem.* **2005**, *44*, 4699.

[39] D. G. Billing, A. Lemmerer, *Acta Crystallogr., Sect. B: Struct. Sci.* **2007**, *63*, 735.

[40] C. C. Stoumpos, D. H. Cao, D. J. Clark, J. Young, J. M. Rondinelli, J. I. Jang, J. T. Hupp, M. G. Kanatzidis, *Chem. Mater.* **2016**, *28*, 2852.

[41] J. Hu, I. W. H. Ostwald, S. J. Stuard, M. M. Nahid, N. Zhou, O. F. Williams, Z. Guo, L. Yan, H. Hu, Z. Chen, X. Xiao, Y. Lin, Z. Yang, J. Huang, A. M. Moran, H. Ade, J. R. Neilson, W. You, *Nat. Commun.* **2019**, *10*, 1276.

[42] F. Zhang, D. H. Kim, H. Lu, J.-S. Park, B. W. Larson, J. Hu, L. Gao, C. Xiao, O. G. Reid, X. Chen, Q. Zhao, P. F. Ndione, J. J. Berry, W. You, A. Walsh, M. C. Beard, K. Zhu, *J. Am. Chem. Soc.* **2019**, *141*, 5972.